Impact of Nuclear Deformation and Pairing on the Charge Radii of Palladium Isotopes

S. Geldhof,[1,2,*] M. Kortelainen,[1,†] O. Beliuskina,[1] P. Campbell,[3] L. Caceres,[4] L. Cañete,[1] B. Cheal,[5] K. Chrysalidis,[6] C. S. Devlin,[5] R. P. de Groote,[1] A. de Roubin,[1] T. Eronen,[1] Z. Ge,[1] W. Gins,[1] A. Koszorus,[5] S. Kujanpää,[1] D. Nesterenko,[1] A. Ortiz-Cortes,[1,4] I. Pohjalainen,[1,7] I. D. Moore,[1] A. Raggio,[1] M. Reponen,[1] J. Romero,[1,5] and F. Sommer[8]

[1]*Accelerator Laboratory, Department of Physics, University of Jyväskylä, 40014 Jyväskylä, Finland*
[2]*KU Leuven, Instituut voor Kern- en Stralingsfysica, 3001 Leuven, Belgium*
[3]*Department of Physics and Astronomy, University of Manchester, Manchester M13 9PL, United Kingdom*
[4]*Grand Accélérateur National d'Ions Lourds (GANIL), CEA/DSM-CNRS/IN2P3, 14000 Caen, France*
[5]*Department of Physics, University of Liverpool, Liverpool L69 7ZE, United Kingdom*
[6]*CERN, 1217 Geneva, Switzerland*
[7]*GSI Helmholtzzentrum für Schwerionenforschung GmbH, 64291 Darmstadt, Germany*
[8]*Institut für Kernphysik, Technische Universität Darmstadt, 64289 Darmstadt, Germany*

(Received 29 October 2021; revised 1 February 2022; accepted 10 March 2022; published 12 April 2022)

The impact of nuclear deformation can been seen in the systematics of nuclear charge radii, with radii generally expanding with increasing deformation. In this Letter, we present a detailed analysis of the precise relationship between nuclear quadrupole deformation and the nuclear size. Our approach combines the first measurements of the changes in the mean-square charge radii of well-deformed palladium isotopes between $A = 98$ and $A = 118$ with nuclear density functional calculations using Fayans functionals, specifically Fy(std) and Fy(Δr, HFB), and the UNEDF2 functional. The changes in mean-square charge radii are extracted from collinear laser spectroscopy measurements on the $4d^9 5s\,{}^3D_3 \rightarrow 4d^9 5p\,{}^3P_2$ atomic transition. The analysis of the Fayans functional calculations reveals a clear link between a good reproduction of the charge radii for the neutron-rich Pd isotopes and the overestimated odd-even staggering: Both aspects can be attributed to the strength of the pairing correlations in the particular functional which we employ.

DOI: 10.1103/PhysRevLett.128.152501

Nuclear charge radii are an important probe for nuclear structure [1], providing information on, e.g., nuclear shapes, deformation, and shape coexistence [2–5], proton-neutron pairing correlations [6], and the presence of nuclear shell closures [7,8]. In recent years, measurements of nuclear charge radii have also proven exceptionally potent in testing state-of-the-art nuclear density functional theory (DFT) and *ab initio* approaches [9–12], and have furthermore been linked to the properties of infinite nuclear matter and radii of neutron stars [13,14]. Many of these studies involve calculations with Fayans energy density functionals (EDFs) [15].

Fayans EDFs have a density gradient term in the pairing functional, with several parametrizations developed over the years. One of the recent forms is Fy(std) [15], where this term is practically inactive due to the particular dataset used to fit the parameters. To remedy this, a new parametrization Fy(Δr, BCS) was developed, including differential charge radii of calcium isotopes in the parameter adjustment, which has recently been applied to Cd isotopes [16]. This EDF was reoptimized within the Hartree-Fock-Bogoliubov (HFB) framework, resulting in the new Fy(Δr, HFB) EDF [10,17]. It has been applied successfully to describe the charge radii of weakly bound proton-rich Ca nuclei [10]; to reproduce the kinks in the charge radii of Sn isotopes at the $N = 82$ shell closure [7] and in the charge radii of Ag isotopes at $N = 50$ [18]; to investigate the odd-even staggering (OES) in the charge radii of Cu isotopes [11]; and to reproduce the charge radii of K isotopes [12]. So far, all of these studies were performed close to shell closures, and thus in (mainly) spherical nuclei.

In this Letter, Fayans EDFs are used to study deformed open shell nuclei, offering the opportunity to investigate the interplay between nuclear quadrupole deformation and pairing correlations, and the size of atomic nuclei. This presents the first such detailed study with Fayans functionals. An intuitive link between quadrupole deformation and the nuclear mean-square charge radii can be expressed using a semiclassical liquid droplet model approach:

$$\langle r^2 \rangle \approx \langle r^2_{\mathrm{sph}} \rangle \left(1 + \frac{5}{4\pi} \langle \beta_2^2 \rangle \right) \tag{1}$$

with $\langle r^2_{\mathrm{sph}} \rangle$ being the mean-square charge radius of a spherical nucleus with the same volume [19]. This relation shows the quadratic sensitivity of nuclear radii to the underlying nuclear quadrupole deformation. To obtain

better insight into this relationship, we used high-resolution collinear laser spectroscopy to determine the changes in the mean-square charge radii of the $^{98-102,104-106,108,110,112,114,116,118}$Pd isotopes, which presents the first optical spectroscopy of radioactive palladium isotopes. These isotopes are known to be deformed, although there is disagreement on the origin and character of the (possible) change in deformation [20–24].

The refractory character of palladium requires the use of a chemically insensitive production technique. In this work, we used the ion-guide method of radioactive ion beam production [25]. Neutron-rich palladium isotopes ($A > 110$, $N > 64$) were produced via a fission reaction with a 30-MeV proton beam impinging on a thin foil of thorium. Neutron-deficient isotopes were produced in a separate experiment via fusion-evaporation reactions, namely, $^{103}\mathrm{Rh}(p, xn)^{100,101}$Pd with 35-MeV protons, and $^{102}\mathrm{Pd}(p, pxn)^{98,99}$Pd with 60- and 50-MeV protons, respectively. In both cases, the recoiling reaction products were thermalized in fast flowing helium gas, electrostatically guided through a radio frequency sextupole ion guide [26], accelerated to 30 keV, and mass separated using a dipole magnet. Ions were accumulated and cooled in a radio frequency quadrupole (RFQ) cooler buncher [27] and ejected as bunches with a temporal spread of ~ 15 μs toward the collinear laser spectroscopy station [28,29]. Typical ion yields at the end of the beamline were 8000/s at $A = 118$ and 10 500/s at $A = 99$. Stable palladium beams for reference scans of ^{108}Pd were provided by the spark discharge ion source in the off-line station [30] used for all radioactive species except for ^{98,99}Pd. For the latter, a reference beam of ^{102}Pd was used, produced as target knockout material.

Since there were no suitable transitions in the ionic state, a charge-exchange cell (CEC) was used in order to neutralize the ion bunches via electron capture reactions with a potassium vapor. A high neutralization efficiency of about 40% was observed for palladium, with most of the ions neutralizing into the $4d^9 5s\,^3D_3$ state at 6564.15 cm^{-1} [31]. Spectroscopy was performed on the atomic transition from this state to the $4d^9 5p\,^3P_2$ state. The 363.6-nm light was provided by a continuous-wave, frequency-doubled Ti:sapphire laser, which was frequency stabilized to a HighFinesse WSU-10 wave meter. The laser light was focused and overlapped anticollinearly with the atom bunches in front of a photomultiplier tube. A tuning voltage was applied to the CEC to Doppler shift the apparent frequency of the laser light, giving rise to a laser frequency scan across the atomic resonances.

For each scan, the voltage was converted to frequency in the rest frame of the atoms using the recorded laser frequency, calibrated tuning voltage, and RFQ cooler-buncher voltage, adding an offset of 15 V to the latter, which is needed for proper beam energy calibration [28]. The resulting spectra were then fitted with a hyperfine

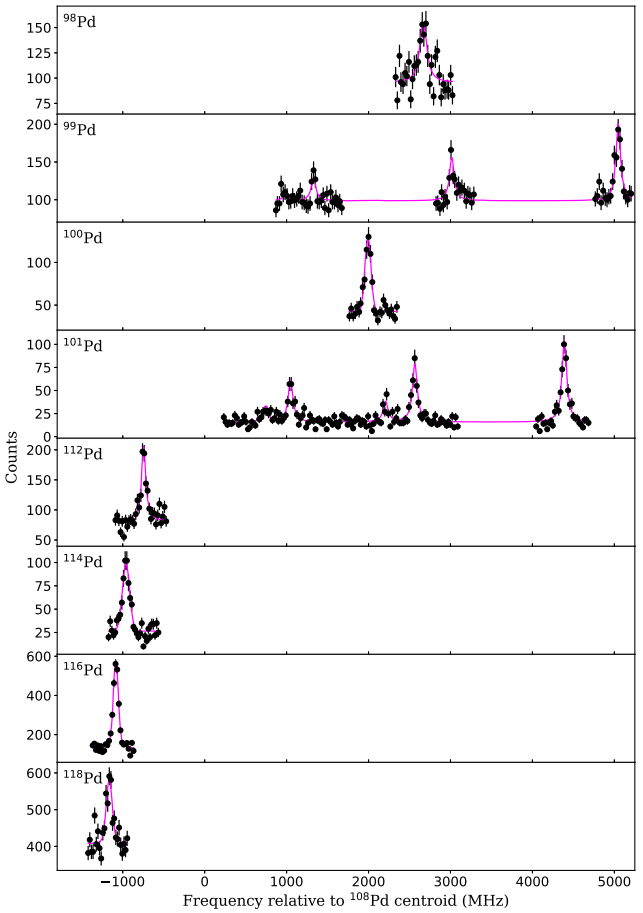

FIG. 1. Optical spectra obtained for all measured radioactive Pd isotopes. The hyperfine structure fits for the odd-A cases and the single peak fits for the even-A, all using Voigt profiles, are shown in pink.

structure fit using Voigt profiles employing a χ^2 minimization routine from the SATLAS package [32]; see Fig. 1. Symmetric Voigt profiles could be used for the fitting, as no skewing of the resonances was observed, a feature observed elsewhere due to the charge-exchange process [33]. In the radioactive odd-A spectra, 5 hyperfine components out of 14 were resolved for ^{101}Pd, as shown in Fig. 1, and 4 components for ^{99}Pd. This was sufficient to constrain the hyperfine structure fit using SATLAS with the ratio of the hyperfine A and B parameters fixed to the ratios of the stable ^{105}Pd isotope, namely, $A_u/A_l = 0.209$ and $B_u/B_l = 0.46$ [31]. Discussion of the fitted hyperfine parameters and resulting nuclear moments is beyond the scope of this work and will be published in a forthcoming paper. The typical FWHM obtained from fitting is around 80–90 MHz for all isotopes, indicating additional broadening on top of the natural linewidth (20 MHz). From the fitted centroids in all spectra, the isotope shifts relative to the centroid of the reference isotope ^{108}Pd were determined. For ^{98,99}Pd, this was done first relative to the reference ^{102}Pd, and then calculating the isotope shifts relative to ^{108}Pd using the

TABLE I. Isotope shifts and resulting changes in mean-square charge radii for all studied isotopes. Statistical errors are shown in round brackets, systematic errors due to voltage determination in square brackets, systematic errors due to wave meter readout (when laser stabilization set point change was necessary) in angled brackets, and systematic errors due to atomic factors in curly brackets. Results for stable isotopes reanalyzed from Ref. [31] using the corrected beam energy. A −2.6% contribution from higher order radial moments has been assumed in the extraction of $\delta\langle r^2\rangle^{108,A}$.

A	$\delta\nu^{108,A}$ (MHz)	$\delta\langle r^2\rangle^{108,A}$ (fm^2)
98	2675(12)[13]	−1.231(4)[4]{13}
99	2451(18)[10]	−1.121(6)[3]{15}
100	1993(4)[25]	−0.929(1)[9]{8}
101	1790(7)[21]	−0.827(2)[7]{8}
102	1452.8(7)[190]	−0.6782(2)[66]{59}
104	958.1(6)[130]	−0.4464(2)[45]{38}
105	839.7(9)[100]	−0.3769(3)[35]{90}
106	494.7(6)[60]	−0.2277(2)[21]{24}
108	0.0	0.0
110	−436.4(8)[60]	0.2052(3)[21]{22}
112	−738(13)[13]⟨10⟩	0.361(4)[4]⟨3⟩{11}
114	−962(13)[13]⟨10⟩	0.487(5)[4]⟨3⟩{24}
116	−1080(14)[12]⟨10⟩	0.574(5)[4]⟨3⟩{44}
118	−1164(13)[18]⟨10⟩	0.648(5)[6]⟨3⟩{65}

known isotope shift $\delta\nu^{108,102}$. These isotope shifts are related to the changes in mean-square charge radii as follows:

$$\delta\nu^{A,A'} = \nu^{A'} - \nu^{A} = FK\delta\langle r^2\rangle^{A,A'} + M\frac{m_{A'} - m_A}{m_{A'}m_A}, \quad (2)$$

where F and M are the electronic field-shift and mass-shift constants of the transition, respectively. These were determined to be $F = -2.9(5)$ GHz/fm^2 and $M = 845(669)$ GHz amu via a King plot procedure in previous work [31]. The factor K corrects for higher order radial moments, the contribution of which can be determined from muonic atom and electron scattering data available for the stable isotopes. For the Pd chain, $K = 0.974$, constituting a −2.6% correction [34].

Table I lists all measured isotope shifts and the resulting changes in mean-square charge radii. The uncertainty on the readout of the tuning and RFQ cooler voltages, 0.1% and 0.01%, respectively [2,35], introduce a systematic scaling error on the isotope shifts [36]. A second fixed systematic error of 10 MHz due to the uncertainty of the WSU-10 wave meter [37] is furthermore included on the values for the neutron-rich isotopes ^{112,114,116,118}Pd, as the laser stabilization set point was changed from that used for the reference isotope ^{108}Pd due to experimental constraints. Finally, the uncertainty on the atomic factors leads to a systematic error on the changes in mean-square charge radii calculated taking into account the correlation

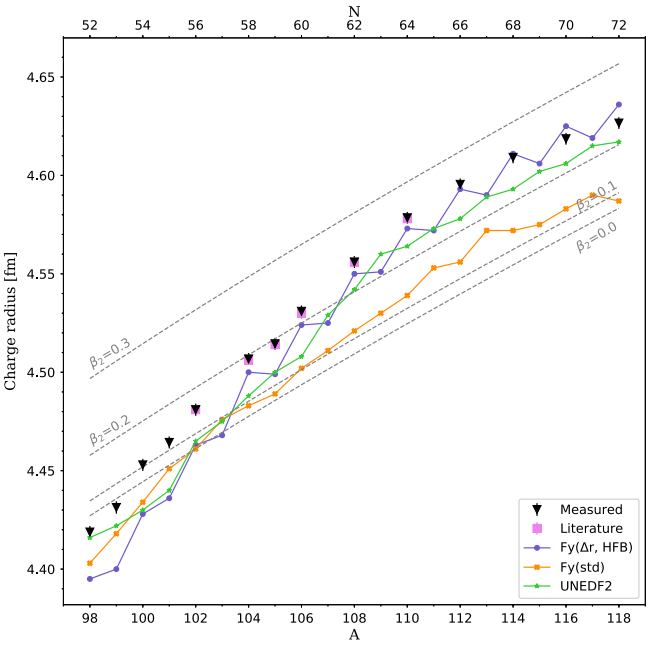

FIG. 2. Evolution of the nuclear charge radii along the palladium isotopic chain from this work, literature [34], and from nuclear DFT calculations using the Fayans Fy(Δr, HFB), Fy(std), and the Skyrme UNEDF2 EDFs. Liquid droplet model [38] isodeformation lines for various values of the deformation parameter β_2 are indicated. Error bars on measured values represent the statistical errors.

between F and M. The experimental results are summarized graphically in Fig. 2. Absolute charge radii were calculated using the radius of ^{108}Pd determined from the combined analysis of muonic x-ray and elastic electron scattering data, $r_{108} = 4.556(3)$ fm [34]. This figure illustrates how the radii increase smoothly as a function of the number of neutrons in the nucleus, with a gradual reduction in the slope when going toward ^{118}Pd. A small OES is also observed.

To compare the measured charge radii to theoretical predictions, we have used the UNEDF2 Skyrme EDF model [39] and Fy(std) and Fy(Δr, HFB) Fayans EDF models in our nuclear structure calculations. The calculations were performed within the HFB framework by assuming an axially symmetric solution. All calculations with UNEDF2 EDF were carried out with the computer code HFBTHO [40] by using a basis consisting of 20 major harmonic oscillator shells. For the Fayans EDF calculations, a modified version of the HFBTHO code was used with the same basis size. The odd-N isotopes were calculated by using quasiparticle blocking with the equal filling approximation [41]. Since the original Fy(std) and Fy(Δr, HFB) EDFs were adjusted with a coordinate space code, the pairing strength parameters needed to be readjusted for the basis-based code. This is due to a much higher density of states in the quasiparticle continuum with the coordinate space approach, leading to a notably different pairing tensor

compared to the basis-based approach. The adjustment was done by scaling all pairing channel EDF parameters with the same coefficient in order to reproduce the neutron pairing gap obtained from the three-point odd-even mass staggering formula [42] in the midshell $N = 70$ Pd isotope. We consider this as a local adjustment for nuclei in the vicinity of the Pd isotopes in the nuclear chart, although we note that calculated charge radii for Ca isotopes in a slightly smaller oscillator basis with current parameters provide good correspondence to experimental values. The zero-range nature of the employed pairing interaction requires a regularization. A standard procedure is to limit the used quasiparticle states up to a certain energy cutoff; see discussion in Ref. [43]. Here, a 60-MeV cutoff was used.

The theoretical calculations for the absolute charge radii are compared to the experimental values in Fig. 2. We also present a comparison to the liquid droplet model of Eq. (1) for different values of the quadrupole deformation parameter β_2. For the calculations using the liquid droplet model, the spherical radius was calculated using the parametrization from Ref. [38] normalized to the charge radius of the reference ^{108}Pd. This comparison illustrates the (likely) change in deformation size along the chain and the quadratic dependence on β_2, but does not provide further insight. The comparison to nuclear DFT on the other hand provides more details. Overall, all functionals describe the correct general smooth parabolic behavior of the measured radii, but Fy(std) underestimates the absolute charge radii, especially with respect to the neutron-rich isotopes. Fy$(\Delta r, \mathrm{HFB})$ is the only functional which reproduces the correct direction of the OES pattern where measured values are available, although the staggering is overestimated somewhat, a feature which has also been observed in other isotopic chains [11,12,16,18]. The other two functionals tend to underestimate the staggering or even show reversed OES compared to the measured values, and also in the predictions for other odd-A isotopes.

To investigate the relationship between deformation, pairing gaps, and nuclear charge radii of the two Fayans functionals more closely, Fig. 3 shows the calculated deformation energy curves, charge radii, and pairing gaps as a function of the quadrupole deformation parameter β_2 for ^{104}Pd and ^{118}Pb. As Figs. 3(a) and 3(d) show, these isotopes have a rather soft deformation character evidenced by the shallow minimum of the deformation energy curves. Our calculations predict similar softness in other open shell palladium isotopes as well; see Supplemental Material [44] for the plots of all studied even-A isotopes. In Figs. 3(b) and 3(e), the dependence of the charge radius on the quadrupole deformation parameter β_2 is shown for ^{104,118}Pd. The results of Fy(std) seem to follow rather closely the parabolic trend of Eq. (1), which is derived from the semiclassical picture. This, however, is not the case with the Fy$(\Delta r, \mathrm{HFB})$ functional. Recall that this functional provides the best overall description of the trend in the charge radii as well as the OES. Figures 3(b) and 3(e) show that with a smaller quadrupole deformation, close to sphericity, the charge radius calculated with Fy$(\Delta r, \mathrm{HFB})$ deviates from the parabolic trend toward higher values. Only for sufficiently large deformation is the parabolic trend mostly restored. This behavior of both Fy(std) and Fy$(\Delta r, \mathrm{HFB})$ is seen in all other isotopes (see Supplemental Material [44]). It is instructive to note a correlation between these charge radius trends and the trend in

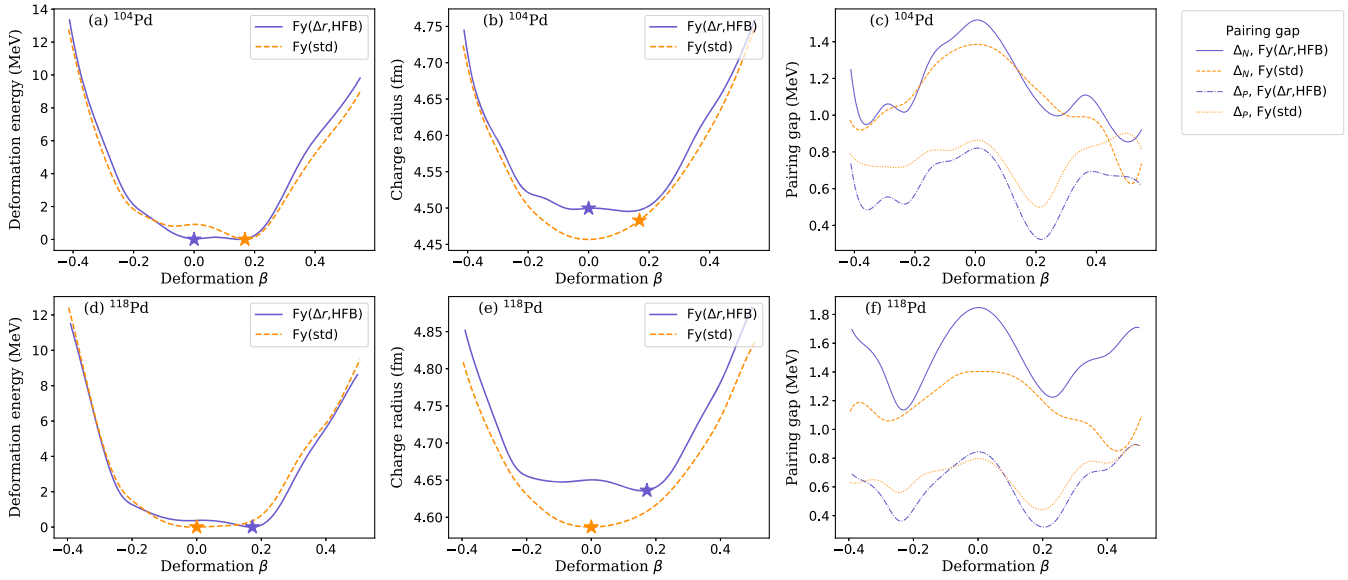

FIG. 3. Calculated quadrupole deformation energy curve (a), calculated charge radius r_{ch} (b), and neutron pairing gap Δ_N and proton pairing gap Δ_P (c) for ^{104}Pd, and the same for ^{118}Pd (d)–(f), with Fy(std) and Fy$(\Delta r, \mathrm{HFB})$ functionals, all as a function of quadrupole deformation parameter β. The star symbols mark the positions of the unconstrained HFB energy minimum.

the pairing gaps, which are shown in Figs. 3(c) and 3(f). The calculated pairing gaps are a good measure of the amount of pairing correlations in the HFB solution. The strong coupling in the pairing part of the Fy(Δr, HFB) functional, which combines the gradient term of normal density and the pairing density, explains the deviation from the simple parabolic relationship: Strong pairing correlations modify the nuclear mean field more at the surface, leading to a larger charge radius. The same coupling also leads to the enhanced OES of the charge radius: In odd-N isotopes, the blocking of the odd particle orbital leads to a reduced strength of the pairing correlations, and, hence, to smaller radii.

In conclusion, this work presented the first optical spectroscopy of short-lived palladium isotopes, allowing the extraction of changes in mean-square charge radii. These were compared to nuclear DFT calculations using the Skyrme UNEDF2 functional and two Fayans functionals, Fy(std) and Fy(Δr, HFB), providing the first detailed investigation of the Fayans functionals in calculating charge radii of deformed open shell nuclei. The particular pairing functional of Fy(Δr, HFB) leads to a good reproduction of the charge radii of the midshell neutron-rich isotopes, even though the charge radii of the neutron-deficient isotopes are slightly underestimated. At the same time, it is also responsible for the correct sign but overestimation of the OES. This highlights the subtle interplay between various nuclear properties in reproducing different features in the overall trend of nuclear charge radii, as well as local variations therein. It shows the importance of charge radii measurements, including farther away from closed shells, for testing existing theoretical nuclear structure models as well as for the development of new models. The region around $Z = 50$ is of particular interest now that it is becoming accessible to *ab initio* models in addition to density functional theory, with calculations recently performed in tin and neighboring isotopic chains [45–47]. To emphasize, the interplay between pairing correlations, deformation, and charge radius will necessitate the adjustment of Fayans EDF parameters at the deformed HFB level in order to improve the predictive power for open shell nuclei.

We acknowledge the CSC-IT Center for Science Ltd., Finland, for the allocation of computational resources. This work has received funding from the European Union's Horizon 2020 research and innovation program under Grant Agreement No. 654002 (ENSAR2) and from the UK Science and Technology Facilities Council. We acknowledge W. Nörtershäuser for the use of the charge-exchange cell.

*sarina.geldhof@cern.ch
†markus.kortelainen@jyu.fi

[1] P. Campbell, I. D. Moore, and M. R. Pearson, Prog. Part. Nucl. Phys. **86**, 127 (2016).
[2] P. Campbell, H. L. Thayer, J. Billowes, P. Dendooven, K. T. Flanagan, D. H. Forest, J. A. R. Griffith, J. Huikari, A. Jokinen, R. Moore, A. Nieminen, G. Tungate, S. Zemlyanoi, and J. Äystö, Phys. Rev. Lett. **89**, 082501 (2002).
[3] K. T. Flanagan *et al.*, Phys. Rev. Lett. **111**, 212501 (2013).
[4] X. F. Yang *et al.*, Phys. Rev. Lett. **116**, 182502 (2016).
[5] B. A. Marsh *et al.*, Nat. Phys. **14**, 1163 (2018).
[6] M. L. Bissell, J. Papuga, H. Naïdja, K. Kreim, K. Blaum, M. De Rydt, R. F. Garcia Ruiz, H. Heylen, M. Kowalska, R. Neugart, G. Neyens, W. Nörtershäuser, F. Nowacki, M. M. Rajabali, R. Sanchez, K. Sieja, and D. T. Yordanov, Phys. Rev. Lett. **113**, 052502 (2014).
[7] C. Gorges *et al.*, Phys. Rev. Lett. **122**, 192502 (2019).
[8] T. Day Goodacre *et al.*, Phys. Rev. Lett. **126**, 032502 (2021).
[9] R. F. Garcia Ruiz *et al.*, Nat. Phys. **12**, 594 (2016).
[10] A. J. Miller, K. Minamisono, A. Klose, D. Garand, C. Kujawa, J. D. Lantis, Y. Liu, B. Maaß, P. F. Mantica, W. Nazarewicz, W. Nörtershäuser, S. V. Pineda, P.-G. Reinhard, D. M. Rossi, F. Sommer, C. Sumithrarachchi, A. Teigelhöfer, and J. Watkins, Nat. Phys. **15**, 432 (2019).
[11] R. P. de Groote *et al.*, Nat. Phys. **16**, 620 (2020).
[12] Á. Koszorús *et al.*, Nat. Phys. **17**, 439 (2021).
[13] G. Hagen, A. Ekström, C. Forssén, G. R. Jansen, W. Nazarewicz, T. Papenbrock, K. A. Wendt, S. Bacca, N. Barnea, B. Carlsson, C. Drischler, K. Hebeler, M. Hjorth-Jensen, M. Miorelli, G. Orlandini, A. Schwenk, and J. Simonis, Nat. Phys. **12**, 186 (2016).
[14] S. Kaufmann *et al.*, Phys. Rev. Lett. **124**, 132502 (2020).
[15] P.-G. Reinhardand and W. Nazarewicz, Phys. Rev. C **95**, 064328 (2017).
[16] M. Hammen *et al.*, Phys. Rev. Lett. **121**, 102501 (2018).
[17] P.-G. Reinhard, W. Nazarewicz, and R. F. Garcia Ruiz, Phys. Rev. C **101**, 021301(R) (2020).
[18] M. Reponen *et al.*, Nat. Commun. **12**, 4596 (2021).
[19] E. W. Otten, in *Treatise on Heavy-Ion Science*, edited by D. A. Bromley (Springer, Boston, 1989), Vol. 8, pp. 517–638.
[20] M. Houry *et al.*, Eur. Phys. J. A **6**, 43 (1999).
[21] D. Fong *et al.*, Phys. Rev. C **72**, 014315 (2005).
[22] J. Kurpeta, W. Urban, A. Płochocki, J. Rissanen, V.-V. Elomaa, T. Eronen, J. Hakala, A. Jokinen, A. Kankainen, P. Karvonen, I. D. Moore, H. Penttilä, S. Rahaman, A. Saastamoinen, T. Sonoda, J. Szerypo, C. Weber, and J. Äystö, Phys. Rev. C **82**, 027306 (2010).
[23] J. Kurpeta, A. Płochocki, W. Urban, T. Eronen, A. Jokinen, A. Kankainen, V. S. Kolhinen, I. D. Moore, H. Penttilä, M. Pomorski, S. Rinta-Antila, and T. Rząca-Urban, and J. Wiśniewski, Phys. Rev. C **98**, 024318 (2018).
[24] H. Hua, C. Y. Wu, D. Cline, A. B. Hayes, R. Teng, R. M. Clark, P. Fallon, A. Goergen, A. O. Macchiavelli, and K. Vetter, Phys. Lett. B **562**, 201 (2003).
[25] I. D. Moore, P. Dendooven, and J. Ärje, Hyperfine Interact. **223**, 17 (2014).
[26] P. Karvonen, I. D. Moore, T. Sonoda, T. Kessler, H. Penttilä, K. Peräjärvi, P. Ronkanen, and J. Äystö, Nucl. Instrum. Methods Phys. Res., Sect. B **266**, 4794 (2008).
[27] A. Nieminen, J. Huikari, A. Jokinen, J. Äystö, P. Campbell, and E. C. A. Cochrane, Nucl. Instrum. Methods Phys. Res., Sect. A **469**, 244 (2001).

[28] R. P. de Groote, A. de Roubin, P. Campbell, B. Cheal, C. S. Devlin, T. Eronen, S. Geldhof, I. D. Moore, M. Reponen, S. Rinta-Antila, and M. Schuh, Nucl. Instrum. Methods Phys. Res., Sect. B **463**, 437 (2020).
[29] L. J. Vormawah, M. Vilén, R. Beerwerth, P. Campbell, B. Cheal, A. Dicker, T. Eronen, S. Fritzsche, S. Geldhof, A. Jokinen, S. Kelly, I. D. Moore, M. Reponen, S. Rinta-Antila, S. O. Stock, and A. Voss, Phys. Rev. A **97**, 042504 (2018).
[30] M. Vilén, L. Canete, B. Cheal, A. Giatzoglou, R. de Groote, A. de Roubin, T. Eronen, S. Geldhof, A. Jokinen, A. Kankainen, I. D. Moore, D. A. Nesterenko, H. Penttilä, I. Pohjalainen, M. Reponen, and S. Rinta-Antila, Nucl. Instrum. Methods Phys. Res., Sect. B **463**, 382 (2020).
[31] S. Geldhof, P. Campbell, B. Cheal, R. P. de Groote, W. Gins, and I. D. Moore, Hyperfine Interact. **241**, 41 (2020).
[32] W. Gins, R. P. de Groote, M. Bissell, C. G. Buitrago, R. Ferrer, K. M. Lynch, G. Neyens, and S. Sels, Comput. Phys. Commun. **222**, 286 (2018).
[33] A. Klose, K. Minamisono, C. Geppert, N. Frömmgen, M. Hammen, J. Krämer, A. Krieger, C. D. P. Levy, P. F. Mantica, W. Nörtershäuser, and S. Vinnikova, Nucl. Instrum. Methods Phys. Res., Sect. A **678**, 114 (2012).
[34] G. Fricke and K. Heilig, *Nuclear Charge Radii* (Landolt-Börnstein/Springer, Berlin, 2004).
[35] F. C. Charlwood, K. Baczynska, J. Billowes, P. Campbell, B. Cheal, T. Eronen, D. H. Forest, A. Jokinen, T. Kessler, I. D. Moore, H. Penttilä, R. Powis, M. Rüffer, A. Saastamoinen, G. Tungate, and J. Äystö, Phys. Lett. B **674**, 23 (2009).
[36] A. Voss, V. Sonnenschein, P. Campbell, B. Cheal, T. Kron, I. D. Moore, I. Pohjalainen, S. Raeder, N. Trautmann, and K. Wendt, Phys. Rev. A **95**, 032506 (2017).
[37] M. Verlinde, K. Dockx, S. Geldhof, K. König, D. Studer, T. E. Cocolios, R. P. de Groote, R. Ferrer, Y. Kudryavtsev, T. Kieck, I. Moore, W. Nörtershäuser, S. Raeder, P. Van den Bergh, P. Van Duppen, and K. Wendt, Appl. Phys. B **126**, 85 (2020).
[38] P. Möller, W. D. Myers, H. Sagawa, and S. Yoshida, Phys. Rev. Lett. **108**, 052501 (2012).
[39] M. Kortelainen, J. McDonnell, W. Nazarewicz, E. Olsen, P.-G. Reinhard, J. Sarich, N. Schunck, S. M. Wild, D. Davesne, J. Erler, and A. Pastore, Phys. Rev. C **89**, 054314 (2014).
[40] M. Stoitsov, N. Schunck, M. Kortelainen, N. Michel, H. Nam, E. Olsen, J. Sarich, and S. Wild, Comput. Phys. Commun. **184**, 1592 (2013).
[41] S. Perez-Martinand and L. M. Robledo, Phys. Rev. C **78**, 014304 (2008).
[42] W. Satuła, J. Dobaczewski, and W. Nazarewicz, Phys. Rev. Lett. **81**, 3599 (1998).
[43] J. Dobaczewski, H. Flocard, and J. Treiner, Nucl. Phys. **A422**, 103 (1984).
[44] See Supplemental Material at http://link.aps.org/supplemental/10.1103/PhysRevLett.128.152501 for theoretical calculations as a function of quadrupole deformation parameter β for all even-A isotopes.
[45] T. D. Morris, J. Simonis, S. R. Stroberg, C. Stumpf, G. Hagen, J. D. Holt, G. R. Jansen, T. Papenbrock, R. Roth, and A. Schwenk, Phys. Rev. Lett. **120**, 152503 (2018).
[46] P. Gysbers, G. Hagen, J. D. Holt, G. R. Jansen, T. D. Morris, P. Navrátil, T. Papenbrock, S. Quaglioni, A. Schwenk, S. R. Stroberg, and K. A. Wendt, Nat. Phys. **15**, 428 (2019).
[47] V. Manea *et al.*, Phys. Rev. Lett. **124**, 092502 (2020).